INTERNATIONAL JOURNAL FOR NUMERICAL METHODS IN FLUIDS
Int. J. Numer. Meth. Fluids 2007; **53**:57–80
Published online 19 June 2006 in Wiley InterScience (www.interscience.wiley.com). DOI: 10.1002/fld.1248

Higher-order bounded differencing schemes for compressible and incompressible flows

K. C. Ng[1,*,†], M. Z. Yusoff[1,‡] and E. Y. K. Ng[2,§]

[1]*Department of Mechanical Engineering, Universiti Tenaga Nasional, Km. 7, Jalan Kajang-Puchong, 43009 Kajang, Selangor Darul Ehsan, Malaysia*
[2]*School of Mechanical and Aerospace Engineering, Nanyang Technological University, 50 Nanyang Avenue, Singapore 639798, Singapore*

SUMMARY

In recent years, three higher-order (HO) bounded differencing schemes, namely AVLSMART, CUBISTA and HOAB that were derived by adopting the normalized variable formulation (NVF), have been proposed. In this paper, a comparative study is performed on these schemes to assess their numerical accuracy, computational cost as well as iterative convergence property. All the schemes are formulated on the basis of a new dual-formulation in order to facilitate their implementations on unstructured meshes. Based on the proposed dual-formulation, the net effective blending factor (NEBF) of a high-resolution (HR) scheme can now be measured and its relevance on the accuracy and computational cost of a HR scheme is revealed on three test problems: (1) advection of a scalar step-profile; (2) 2D transonic flow past a circular arc bump; and (3) 3D lid-driven incompressible cavity flow. Both density-based and pressure-based methods are used for the computations of compressible and incompressible flow, respectively. Computed results show that all the schemes produce solutions which are nearly as accurate as the third-order QUICK scheme; however, without the unphysical oscillations which are commonly inherited from the HO linear differencing scheme. Generally, it is shown that at higher value of NEBF, a HR scheme can attain better accuracy at the expense of computational cost. Copyright © 2006 John Wiley & Sons, Ltd.

Received 23 January 2006; Revised 30 March 2006; Accepted 31 March 2006

KEY WORDS: high-resolution scheme; normalized variable formulation; boundedness; time-marching method; SIMPLE; QUICK

*Correspondence to: K. C. Ng, Department of Mechanical Engineering, Universiti Tenaga Nasional, Km. 7, Jalan Kajang-Puchong, 43009 Kajang, Selangor Darul Ehsan, Malaysia.
†E-mail: ngkhaiching2000@yahoo.com
‡E-mail: zamri@uniten.edu.my
§E-mail: MYKNG@ntu.edu.sg

Contract/grant sponsor: Ministry of Science Technology and Innovation (MOSTI), Malaysia; contract/grant number: 09-99-03-0013-EA001
Contract/grant sponsor: UNITEN; contract/grant number: J510010026

1. INTRODUCTION

Successful computation of convection–diffusion problem is one of the most challenging research areas in computational fluid dynamics (CFD), which attracts many CFD researchers to work towards the 'perfect' discretization scheme since the past few decades. For the numerical discretization of diffusive term, second-order central differencing (CD) works very well and is almost commonly adopted in most of the engineering simulations.

For the convective terms that are invariably present in the flow governing equations, development of an efficient differencing scheme which is easy to implement but is free of false diffusion has become one of the difficult tasks among the CFD community. Although the classical schemes such as the first-order upwind differencing (UD), the hybrid central/upwind scheme (HYRBID) by Patankar [1] and the POWER-LAW by Spalding [2] are unconditionally bounded and highly stable, they tend to produce unsatisfactory results in most of the cases due to the excessive generation of numerical diffusion when the flow direction is skewed relative to the grid line. To overcome the false diffusions associated with these schemes, the straightforward remedy is to use a fine grid; however, such an approach is not practical due to huge amount of data storage, thus increasing the CPU time consumption especially in 3D flow computations. Considerable efforts have been made towards the development of a series of improved schemes mainly in two directions. The first attempt is to retain the simplicity of UD; meanwhile, reducing the errors in the regions where the grid line and the velocity direction are not closely aligned as proposed by Raithby [3] in his skew upstream differencing scheme (SUDS). However, it suffers from lack of boundedness and this has motivated Darwish and Moukalled [4] in devising a composite high-resolution (HR) bounded convective scheme making use of the convection boundedness criterion (CBC) [5]. Their normalized variable formulation (NVF) is known as NVF-SUDS and successfully suppressing the unphysical oscillations from the flow solutions. In spite of this, due to the nature of SUDS, which requires tracing of a pair of appropriate upstream nodes, this technique is not readily implemented in unstructured grid environment. The second attempt is to enhance the order of accuracy of the scheme. A variety of so-called higher-order (HO) schemes have been presented and tested over the years such as the second-order upwind scheme of Warming and Beam [6], the quadratic upstream interpolation for convective kinematics (QUICK) scheme by Leonard [7] and the third-order scheme of Agarwal [8]. These schemes have been proven to be successful in increasing the solution accuracy, but all suffer from the boundedness problems, which can induce large errors and lead to unphysical results.

Imposition of the boundedness property to the HO scheme leads to the so-called HR scheme, which allows good resolution of steep gradient without introducing unphysical oscillation in the solution. The earliest effort in devising such a scheme has been attempted by Harten [9] in his total variation diminishing (TVD) technique. In the TVD approach for constructing HR scheme, flux limiter functions, such as SUPERBEE by Roe [10], MINMOD limiter by Sweby [11], and more recently incorporation of MUSCL [12] scheme by Chan and Ng [13] in their modified distribution-formula cell-vertex scheme, have been proposed. Another analogous numerical tool was later introduced by Gaskell and Lau [5] in their sharp and monotonic algorithm for realistic transport (SMART) scheme presented in the form of NVF in which boundedness is guaranteed if CBC is satisfied. A number of previously proposed TVD limiters have been re-interpreted in the form of NVF as shown by Leonard [14] and Zijlema and Wesseling [15], demonstrating that both TVD and NVF schemes use some sort of 'unboundedness sensor' to transform the linear but unbounded HO scheme into a bounded but non-linear HR scheme. Based on the CBC criterion, quite a number of high-resolution NVF schemes have been developed such as the Second-

DOI: 10.1002/fld

Order-Upwind-Central-differencing-first-order-UPwind (SOUCUP) scheme by Zhu and Rodi [16] and some contemporary NVF schemes; for instance, GAMMA by Jasak *et al*. [17], weighted-average coefficient ensuring boundedness (WACEB) by Song *et al*. [18, 19], AVLSMART by Przulj and Basara [20], scheme based on extended CBC (SECBC) by Hou *et al*. [21], convergent and universally bounded interpolation scheme for the treatment of advection (CUBISTA) by Alves *et al*. [22] and χ-schemes by Darwish and Moukalled [23]. Very recently, Hou *et al*. [21] have proven that CBC is only a sufficient condition for a scheme possessing boundedness, and they have proposed another CBC named as the extended CBC (ECBC), which is a sufficient and necessary condition for a bounded scheme to possess at least second-order accuracy. This has given impetus to Wei *et al*. [24] in demonstrating a new differencing scheme based on this ECBC criterion denoted as the high-order-accurate and bounded (HOAB) scheme to preserve boundedness and accuracy for incompressible flow calculations. As reported by Hou *et al*. [21], most of the NVF schemes proposed to date satisfy ECBC, including the schemes considered in the present study.

While a number of bounded HR schemes have been implemented for structured meshes, only few workers have implemented NVF on unstructured grid, partly due to the difficulty in addressing the far-upwind value, which is required in calculating the normalized variable. The addressing issue in unstructured environment by using NVF has been resolved by Jasak *et al*. [17] in their GAMMA scheme by employing only the compact computational molecules (the nearest neighbours of a control volume). Very recently, Woodfield *et al*. [25] have implemented the NVF technique to resolve the issue of boundedness in the context of vertex-centred unstructured finite volume algorithm. Darwish and Moukalled [23] have reconstructed a virtual upwind value based on the normalized formulation given by Jasak *et al*. [17] to achieve HO approximation. From the authors' opinion, due to the fact that the projected upwind value is already implicitly satisfied in the compact formulation proposed by Jasak *et al*. [17] (see Reference [20]), a unified dual-formulation can be retrieved, as will be shown later in this paper.

The objective of this paper is to present a direct comparison of the recently developed higher-order HR schemes, namely CUBISTA, AVLSMART and HOAB on structured and unstructured meshes. The authors also include the solutions of GAMMA due to its common mathematical background as compared to that of the proposed unified dual-formulation denoted as the γ-family of schemes. These schemes, apart from facilitating the implementations of NVF schemes on arbitrary meshes, serve as an attempt to quantify the diffusion level (hence accuracy) of a HR scheme denoted as the net effective blending factor (NEBF) in the current paper. Three test cases are examined: the transport of a passive scalar in a prescribed velocity field, a 2D transonic flow past a circular arc bump and a 3D lid-driven flow in a cubic cavity at two different Reynolds numbers. The calculations are carried out with a finite volume method for compressible and incompressible flow calculations, using density-based method for the first case and pressure-based method for the latter case.

2. NORMALIZED VARIABLE FORMULATION (NVF)

According to Leonard [26], the local flow variable, ϕ can be transformed into its normalized form, $\tilde{\phi}$ defined by

$$\tilde{\phi} = \frac{\phi - \phi_{\mathrm{U}}}{\phi_{\mathrm{D}} - \phi_{\mathrm{U}}} \tag{1}$$

DOI: 10.1002/fld

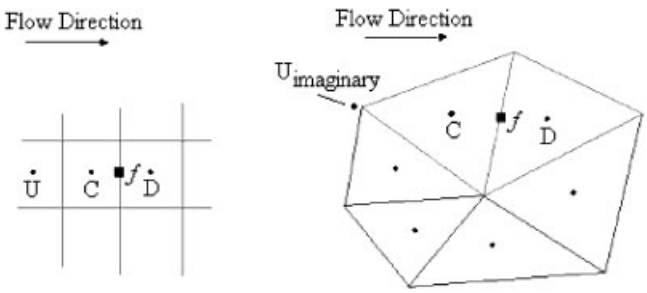

Figure 1. Control volumes for structured (left) and unstructured meshes (right).

where the subscript U represents the upstream value and the subscript D represents the downstream value as illustrated in Figure 1 for both structured and unstructured environments.

It is easy to note that this normalization leads to $\tilde{\phi}_U = 0$ and $\tilde{\phi}_D = 1$, which is helpful in defining the properties of boundedness and monotonicity in the normalized variable diagram (NVD). For instance, in usual (un-normalized) notation, the functional relationships for second-order CD scheme and QUICK scheme by Leonard [7] are given by (for uniform grid)

$$\text{CD: } \phi_f = f(\phi_C, \phi_D) = \tfrac{1}{2}(\phi_C + \phi_D) \tag{2}$$

$$\text{QUICK: } \phi_f = g(\phi_U, \phi_C, \phi_D) = \tfrac{1}{2}(\phi_C + \phi_D) - \tfrac{1}{8}(\phi_D - 2\phi_C + \phi_U) \tag{3}$$

where f and C denote face and local cell value, respectively. Using Equation (1) to normalize the variables in Equations (2) and (3), one will obtain

$$\text{CD: } \tilde{\phi}_f = f(\tilde{\phi}_C) = \tfrac{1}{2} + \tfrac{1}{2}(\tilde{\phi}_C) \tag{4}$$

$$\text{QUICK: } \tilde{\phi}_f = g(\tilde{\phi}_C) = \tfrac{3}{8} + \tfrac{3}{4}(\tilde{\phi}_C) \tag{5}$$

A number of linear schemes written using NVF are given in Table I. It is interesting to note that all the normalized mathematical relationships for these schemes are written as a linear function of $\tilde{\phi}_C$ only and well represented in the form of NVD as depicted in Figure 2. The un-normalized relationships for different schemes are also provided in the same table. As seen, among the un-normalized formulations of the higher-order accurate linear schemes, only CD employs compact computational molecules, which is appropriate for application in unstructured grid environment. This serves as the basis for the numerical framework of γ-family of schemes to be defined in Section 2.1.

The NVD is an attractive tool to assess both the accuracy as well as the diffusivity of numerical schemes. For example, the scheme that has a NVD plot near the UD line ($\tilde{\phi}_f = \tilde{\phi}_C$) tends to be highly diffusive; while the scheme that resides near the downwind line ($\tilde{\phi}_f = 1$) is highly compressive (see Reference [23]). This will be demonstrated quantitatively in Section 3 based on the proposed γ-family of schemes.

DOI: 10.1002/fld

Table I. Mathematical relationships for different linear schemes (UD/HO schemes).

Linear scheme/ base scheme	Usual/un-normalized relationship $f(\phi_U, \phi_C, \phi_D)$	Normalized relationship $g(\tilde{\phi}_C)$	Base scheme for the following HR schemes [23]
First-order upwinding (UD)	$\phi_f = \phi_C$	$\tilde{\phi}_f = \tilde{\phi}_C$	—
Second-order linear upwind differencing (LUD) [6]	$\phi_f = \frac{3\phi_C - \phi_U}{2}$	$\tilde{\phi}_f = \frac{3}{2}\tilde{\phi}_C$	OSHER [27]
Second-order central differencing (CD)	$\phi_f = \frac{1}{2}(\phi_C + \phi_D)$	$\tilde{\phi}_f = \frac{1}{2}\tilde{\phi}_C + \frac{1}{2}$	GAMMA [17]
Fromm's method [28]	$\phi_f = \phi_C + \frac{\phi_D - \phi_U}{4}$	$\tilde{\phi}_f = \frac{1}{4} + \tilde{\phi}_C$	MUSCL [12]
QUICK [7]	$\phi_f = \frac{1}{2}(\phi_C + \phi_D) - \frac{1}{8}(\phi_D - 2\phi_C + \phi_U)$	$\tilde{\phi}_f = \frac{3}{8} + \frac{3}{4}\tilde{\phi}_C$	SMART [5]

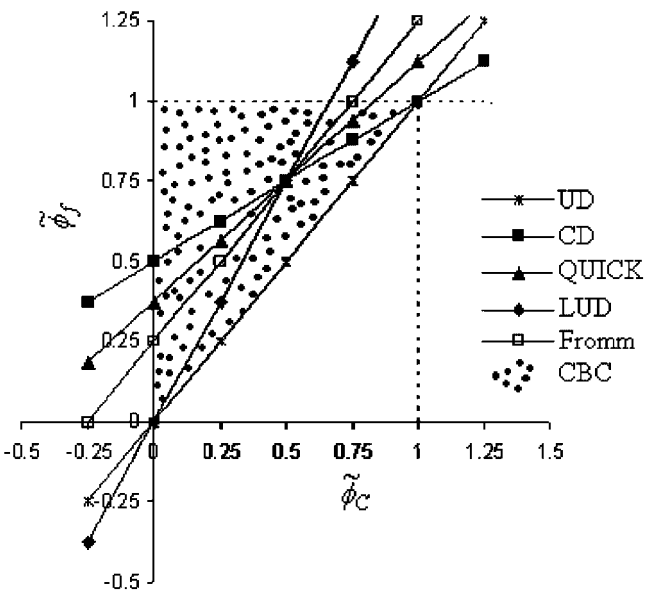

Figure 2. CBC criterion and NVD plots for different linear schemes.

As dictated by Gaskell and Lau [5] in their CBC, a scheme is bounded if its normalized relationship is resided within the region portrayed graphically in Figure 2 for the monotonic range: $0<\tilde{\phi}_C<1$. For region $\tilde{\phi}_C \notin (0, 1)$, the scheme should follow the UD line. The above conditions

DOI: 10.1002/fld

can be formulated as

$$\begin{aligned} \text{CBC: } & \tilde{\phi}_C \leqslant \tilde{\phi}_f \leqslant 1 \quad \text{if } 0 < \tilde{\phi}_C < 1 \\ & \tilde{\phi}_f = \tilde{\phi}_C \quad \text{if } \tilde{\phi}_C \geqslant 1 \text{ or } \tilde{\phi}_C \leqslant 0 \end{aligned} \tag{6}$$

However, it is observed that none of the linear schemes shown in Figure 2 possess the boundedness property for the entire range of $\tilde{\phi}_C$. Therefore, it can be concluded that any differencing scheme that is more than first-order accurate must be non-linear in order to preserve boundedness. As a consequence of the flexibility of CBC expressed in the NVD form, quite a number of non-linear HR schemes have been proposed and tested, such as the well-known MINMOD limiter by Sweby [11], and more recently GAMMA by Jasak *et al*. [17], AVLSMART by Przulj and Basara [20], CUBISTA by Alves *et al*. [22] and HOAB by Wei *et al*. [24], to be considered in the present study.

2.1. The formulations of χ-schemes and γ-schemes

The derivation of γ-family of schemes is motivated from the dual-formulation (χ-schemes) by Darwish and Moukalled [23] in which the normalized equation can be readily/equally written in terms of the un-normalized variables thus facilitating the implementations of any HR scheme on arbitrary grid. The dual-formulation of χ-schemes can be written as

$$\text{Normalized: } \tilde{\phi}_f^{HR} = \tilde{\phi}_C + \chi(\tilde{\phi}_f^{HO} - \tilde{\phi}_C) \tag{7}$$

$$\text{Un-normalized: } \phi_f^{HR} = \phi_C + \chi(\phi_f^{HO} - \phi_C) \tag{8}$$

where $\tilde{\phi}_f^{HO}$ is the base scheme for the formulation of any HR scheme, $\tilde{\phi}_f^{HR}$. For example, the base scheme for SMART (HR) is QUICK (HO). A number of HR schemes with their respective base schemes in χ-formulation are presented in Table I.

By collecting similar terms in Equations (7) and (8), one will obtain

$$\text{Normalized: } \tilde{\phi}_f^{HR} = (1 - \chi)\tilde{\phi}_C + \chi\tilde{\phi}_f^{HO} \tag{9}$$

$$\text{Un-normalized: } \phi_f^{HR} = (1 - \chi)\phi_C + \chi\phi_f^{HO} \tag{10}$$

Hence, χ can be interpreted as the 'blending factor' in which $\phi_f^{HR} = \phi_C$ when $\chi = 0$ and $\phi_f^{HR} = \phi_f^{HO}$ when $\chi = 1$. Clearly, the blending concept presented here is analogous to the expressions proposed by Jasak and his co-workers (cf. Reference [17, Equation (27)]) whereby the base scheme for their GAMMA scheme is essentially CD. The blending factor χ in χ-family of schemes is given by

$$\chi = \frac{\tilde{\phi}_f^{HR} - \tilde{\phi}_C}{\tilde{\phi}_f^{HO} - \tilde{\phi}_C} = h(\tilde{\phi}_C) \tag{11}$$

which is dependent on the local shape of the flow solution, denoted by the normalized variable, $\tilde{\phi}_C$.

As shown in Equation (9), $\tilde{\phi}_f^{HR}$ is principally expressed as a function of $\tilde{\phi}_C$. In order to compute $\tilde{\phi}_C$, ϕ_U is needed which is not naturally defined for unstructured grid. In the localized method

DOI: 10.1002/fld

proposed by Jasak *et al*. [17], however, ϕ_U is not necessary whereby $\tilde{\phi}_C$ is expressed as

$$\tilde{\phi}_C = 1 - \frac{\phi_D - \phi_C}{2(\nabla\phi)_C \cdot \underline{d}} \tag{12}$$

$\underline{d}$ is $\overrightarrow{CD}$ (refer to Figure 1) and $(\nabla\phi)_C$ can be evaluated using the Gauss divergence theorem. Using Equation (12), Darwish and Moukalled [23] have reconstructed the far-upwind value, ϕ_U based on the local cell-gradient

$$\phi_U = \phi_D - 2\nabla\phi_C \cdot \underline{d} \tag{13}$$

in order to achieve HO accuracy by calculating ϕ_f^{HO} in Equation (10), and thus ϕ_f^{HR} can be determined. From the authors' opinion, however, in order to make full use of the flexibility (the localized/compact nature) of Equation (12) for unstructured grid, the reconstruction of the far-upwind value can be neglected since it is already implicitly satisfied in Equation (12), as firstly recognized by Przulj and Basara [20]. Therefore, the main issue here is to select an appropriate base scheme in the dual-formulation so that it uses only a compact computational molecule and hence the reconstruction procedure (gradient-projection) can be omitted for all computational cases. Following this, a dual-formulation unifying the construction of all HR schemes can be revealed.

As shown in Table I, the only choice will be the CD scheme due to its compact nature. Contrary to χ-family of schemes whereby the base schemes may vary from one to another, the proposed γ-schemes enforce consistency by employing CD as the base scheme for the construction of all HR schemes. Equations (9) and (10) may now be re-written as

$$\text{Normalized: } \tilde{\phi}_f^{HR} = (1-\gamma)\tilde{\phi}_C + \gamma\tilde{\phi}_f^{CD} \tag{14}$$

$$\text{Un-normalized: } \phi_f^{HR} = (1-\gamma)\phi_C + \gamma\phi_f^{CD} = \phi_C + \underline{\gamma(\phi_f^{CD} - \phi_C)} \tag{15}$$

and the new blending factor, γ can be expressed as

$$\gamma = \frac{\tilde{\phi}_f^{HR} - \tilde{\phi}_C}{\tilde{\phi}_f^{CD} - \tilde{\phi}_C} = h(\tilde{\phi}_C) \tag{16}$$

By calculating $\tilde{\phi}_C$ from Equation (12), it is now straightforward to evaluate ϕ_f^{HR} using Equation (15). The underlined expression is denoted as the deferred-correction term [29], which is treated as an extra source term in order to maintain the diagonal dominance of the coefficient matrix obtained from the implicit calculation. The γ-formulations of GAMMA, CUBISTA, AVLSMART, and HOAB will be given in the following section.

2.2. The γ-formulations of non-linear HR schemes

In NVF, the mathematical relationships for the following HR schemes are written as

$$\text{GAMMA: } \tilde{\phi}_f^{HR} = \begin{cases} -\tilde{\phi}_C{}^2 + 2\tilde{\phi}_C, & 0 < \tilde{\phi}_C \leqslant \frac{1}{2} \\ \frac{1}{2} + \frac{1}{2}\tilde{\phi}_C, & \frac{1}{2} < \tilde{\phi}_C < 1 \\ \tilde{\phi}_C & \text{elsewhere} \end{cases} \tag{17}$$

DOI: 10.1002/fld

$$\text{CUBISTA: } \tilde{\phi}_{\mathrm{f}}^{\mathrm{HR}} = \begin{cases} \frac{7}{4}\tilde{\phi}_{\mathrm{C}}, & 0<\tilde{\phi}_{\mathrm{C}}\leqslant\frac{3}{8} \\ \frac{3}{8}+\frac{3}{4}\tilde{\phi}_{\mathrm{C}}, & \frac{3}{8}<\tilde{\phi}_{\mathrm{C}}\leqslant\frac{3}{4} \\ \frac{3}{4}+\frac{1}{4}\tilde{\phi}_{\mathrm{C}}, & \frac{3}{4}<\tilde{\phi}_{\mathrm{C}}<1 \\ \tilde{\phi}_{\mathrm{C}} & \text{elsewhere} \end{cases} \tag{18}$$

$$\text{AVLSMART: } \tilde{\phi}_{\mathrm{f}}^{\mathrm{HR}} = \begin{cases} \frac{9}{4}\tilde{\phi}_{\mathrm{C}}, & 0<\tilde{\phi}_{\mathrm{C}}\leqslant\frac{1}{4} \\ \frac{3}{8}+\frac{3}{4}\tilde{\phi}_{\mathrm{C}}, & \frac{1}{4}<\tilde{\phi}_{\mathrm{C}}\leqslant\frac{3}{4} \\ \frac{3}{4}+\frac{1}{4}\tilde{\phi}_{\mathrm{C}}, & \frac{3}{4}<\tilde{\phi}_{\mathrm{C}}<1 \\ \tilde{\phi}_{\mathrm{C}} & \text{elsewhere} \end{cases} \tag{19}$$

$$\text{HOAB: } \tilde{\phi}_{\mathrm{f}}^{\mathrm{HR}} = \begin{cases} \frac{7}{2}\tilde{\phi}_{\mathrm{C}}, & 0<\tilde{\phi}_{\mathrm{C}}\leqslant\frac{1}{6} \\ \frac{1}{2}\tilde{\phi}_{\mathrm{C}}+\frac{1}{2}, & \frac{1}{6}<\tilde{\phi}_{\mathrm{C}}\leqslant\frac{1}{2} \\ \tilde{\phi}_{\mathrm{C}}+\frac{1}{4}, & \frac{1}{2}<\tilde{\phi}_{\mathrm{C}}\leqslant\frac{3}{4} \\ 1, & \frac{3}{4}<\tilde{\phi}_{\mathrm{C}}<1 \\ \tilde{\phi}_{\mathrm{C}} & \text{elsewhere} \end{cases} \tag{20}$$

with the γ-formulation takes the form

$$\gamma = \frac{\tilde{\phi}_{\mathrm{f}}^{\mathrm{HR}}-\tilde{\phi}_{\mathrm{C}}}{\tilde{\phi}_{\mathrm{f}}^{\mathrm{CD}}-\tilde{\phi}_{\mathrm{C}}} = \frac{\tilde{\phi}_{\mathrm{f}}^{\mathrm{HR}}-\tilde{\phi}_{\mathrm{C}}}{\frac{1}{2}-\frac{1}{2}\tilde{\phi}_{\mathrm{C}}} = \frac{2\left(\tilde{\phi}_{\mathrm{f}}^{\mathrm{HR}}-\tilde{\phi}_{\mathrm{C}}\right)}{1-\tilde{\phi}_{\mathrm{C}}} \tag{21}$$

This translates into the following relationships for the γ-formulations, as follows:

$$\text{GAMMA: } \gamma = \begin{cases} 2\tilde{\phi}_{\mathrm{C}}, & 0<\tilde{\phi}_{\mathrm{C}}\leqslant\frac{1}{2} \\ 1, & \frac{1}{2}<\tilde{\phi}_{\mathrm{C}}<1 \\ 0 & \text{elsewhere} \end{cases} \tag{22}$$

$$\text{CUBISTA: } \gamma = \begin{cases} \frac{3}{2}\tilde{\phi}_{\mathrm{C}}/(1-\tilde{\phi}_{\mathrm{C}}), & 0<\tilde{\phi}_{\mathrm{C}}\leqslant\frac{3}{8} \\ (3-2\tilde{\phi}_{\mathrm{C}})/(4-4\tilde{\phi}_{\mathrm{C}}), & \frac{3}{8}<\tilde{\phi}_{\mathrm{C}}\leqslant\frac{3}{4} \\ \frac{3}{2}, & \frac{3}{4}<\tilde{\phi}_{\mathrm{C}}<1 \\ 0 & \text{elsewhere} \end{cases} \tag{23}$$

DOI: 10.1002/fld

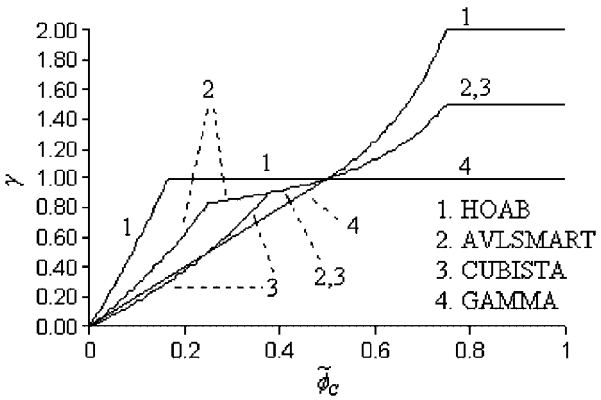

Figure 3. $(\gamma, \tilde{\phi}_C)$ diagrams for HR schemes.

$$\text{AVLSMART: } \gamma = \begin{cases} \frac{5}{2}\tilde{\phi}_C(1-\tilde{\phi}_C), & 0<\tilde{\phi}_C\leqslant\frac{1}{4} \\ (3-2\tilde{\phi}_C)/(4-4\tilde{\phi}_C), & \frac{1}{4}<\tilde{\phi}_C\leqslant\frac{3}{4} \\ \frac{3}{2}, & \frac{3}{4}<\tilde{\phi}_C<1 \\ 0 & \text{elsewhere} \end{cases} \tag{24}$$

$$\text{HOAB: } \gamma = \begin{cases} 5\tilde{\phi}_C/(1-\tilde{\phi}_C), & 0<\tilde{\phi}_C\leqslant\frac{1}{6} \\ 1, & \frac{1}{6}<\tilde{\phi}_C<\frac{1}{2} \\ 1/(2(1-\tilde{\phi}_C)), & \frac{1}{2}<\tilde{\phi}_C\leqslant\frac{3}{4} \\ 2, & \frac{3}{4}<\tilde{\phi}_C<1 \\ 0 & \text{elsewhere} \end{cases} \tag{25}$$

β_m for GAMMA scheme is selected as $\frac{1}{2}$ in the current work. Similar to the $(\chi, \tilde{\phi}_C)$ relationships developed by Darwish and Moukalled [23], the γ-relationships of the above schemes can be visualized on the $(\gamma, \tilde{\phi}_C)$ diagrams as depicted in Figure 3. After computing the γ values from Equations (22)–(25), the interpolated ϕ_f^{HR} can then be determined from Equation (15) without the need of reconstructing the far-upwind value.

3. THE NET EFFECTIVE BLENDING FACTOR (NEBF)

In general, based on the discussions above, the γ-family of schemes can be treated as a class of blended schemes by employing a certain amount of UD ($\gamma = 0$) combined with CD ($\gamma = 1$). A very similar approach has been recently employed by Li and Tao [30] whereby they have used the second-order linear upwind differencing (LUD) as the base scheme and the blending

DOI: 10.1002/fld

Table II. NEBFs for different schemes.

Scheme	NEBF	Boundedness property
First-order upwind differencing (UD)	0.0000	Bounded
MINMOD	0.6931	Bounded
GAMMA	0.7500	Bounded
CUBISTA	0.9341	Bounded
AVLSMART	0.9939	Bounded
Second-order central differencing (CD)	1.0000	Unbounded
SMART	1.1316	Bounded
HOAB	1.2582	Bounded
Downwind differencing (DD)	2.0000	Unbounded

factor γ has been written as a function of local Peclet number instead. In the context of the current work that making use of the normalized variable to construct the blending factor, the HO approximations, such as the HOAB, CUBISTA and AVLSMART schemes can be constructed using the γ-formulation, i.e. Equation (21) by allowing $\gamma>1$ (maximum γ is 2.0000 for downwind differencing) at smooth flow region. In general, the higher value of γ is, the more accurate (less diffusive) the scheme will be. While Peric [31] has used a constant blending factor in his blended differencing (BD) scheme in the entire flow field as contrast to the current γ-formulation whereby variable blending is considered $[\gamma = h(\tilde{\phi}_C)]$, it is appealing to determine the net diffusion level inherited in a HR scheme by judging its NEBF defined as

$$\text{NEBF} = \frac{\int_{S(1)} \gamma_1 \cdot d\tilde{\phi}_C + \int_{S(2)} \gamma_2 \cdot d\tilde{\phi}_C + \cdots + \int_{S(N)} \gamma_N \cdot d\tilde{\phi}_C}{\int_{\forall S} d\tilde{\phi}_C} \tag{26}$$

where $S(N)$ is the segment sequence with N-number of piecewise γ-functions in the monotonic range $(0, 1)$. Physically, the NEBFs for various HR schemes are indeed the areas under their respective $(\gamma, \tilde{\phi}_C)$ diagrams as presented in Figure 3. The NEBFs for different schemes have been presented in Table II, predicting that HOAB is perhaps the most accurate (highest NEBF) HR scheme in the present study, followed by AVLSMART, CUBISTA and GAMMA. The NEBF for SMART scheme is also provided in the same table for comparison purpose, indicating that it is more accurate than its two variants (AVLSMART and CUBISTA); however, it is less accurate than HOAB owing to its lower NEBF as shown in the same table. Following this, it is of interest to note that similar conclusion has been recently reported by Wei *et al*. [24].

4. RESULTS

The four schemes considered in this comparative study have been reformulated as γ-schemes and coded. The calculations performed in this paper are carried out on a HP-workstation (Intel Pentium 4 CPU 2.80 GHz, Memory 512 MB RAM). The compressible flow is computed by a density-based code developed by the authors [32, 33], incorporating a V-cycle multigrid technique as an attempt to accelerate the iterative convergence of the explicit multi-stage Runge–Kutta time-marching solver [34, 35]. For the computation of incompressible flow, the authors have adopted a pressure-based

DOI: 10.1002/fld

code; it uses a non-staggered variable storage technique, which is more robust as compared to the traditional staggered arrangement [36]. Interpolation technique by Rhie and Chow [37] for calculating the mass fluxes at the cell interfaces has been adopted to avoid the pressure oscillations due to the non-staggered arrangement. Pressure–velocity decoupling is resolved via the SIMPLE algorithm by Patankar [1]; further details can be found in Reference [38]. The set of algebraic difference equations are solved with the Gauss–Seidel method whereby the diagonal dominance of the coefficient matrix is ensured via the deferred-correction approach of Khosla and Rubin [29].

4.1. Pure convection of a passive scalar step

The objective of this study is, of course, to test the resolution properties of the HR schemes. The conservation equation to be solved is

$$\nabla \cdot (\underline{U}\phi) = 0 \tag{27}$$

where ϕ is the convective variable and $\underline{U}$ is the velocity vector. For simplicity, the magnitude of the velocity for the pure-convection test problem is assumed to be unity.

Figure 4 illustrates the flow configuration of the well-known pure-convection test problem [24, 38] to show the transportation of a scalar in a uniform oblique velocity field. A step profile is selected.

Single-step profile ($\theta = 30°$):

$$\phi_1(y) = \begin{cases} 0 & \text{for } 0 \leqslant y \leqslant \frac{1}{6} \\ 1 & \text{for } \frac{1}{6} \leqslant y \leqslant 1 \end{cases} \tag{28}$$

$$\phi_2(x) = \{0$$

Calculations are carried out on four uniform grids, comprising of 12×12, 24×24, 36×36 and 48×48 control volumes. A comparison of the scalar profiles at the vertical line $x = 0.5$ is shown in Figures 5(a) and (b) for meshes 12×12 and 48×48, respectively, along with the exact solution. Due to the step profile that provides the stringent gradient variation, the assessment of the scheme's ability to resolve a sharp front with minimum artificial diffusion and oscillation can be performed.

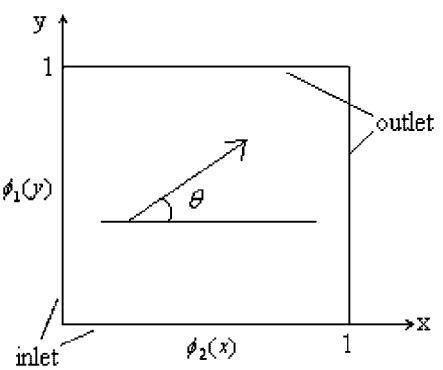

Figure 4. Pure convection in a uniform velocity field.

DOI: 10.1002/fld

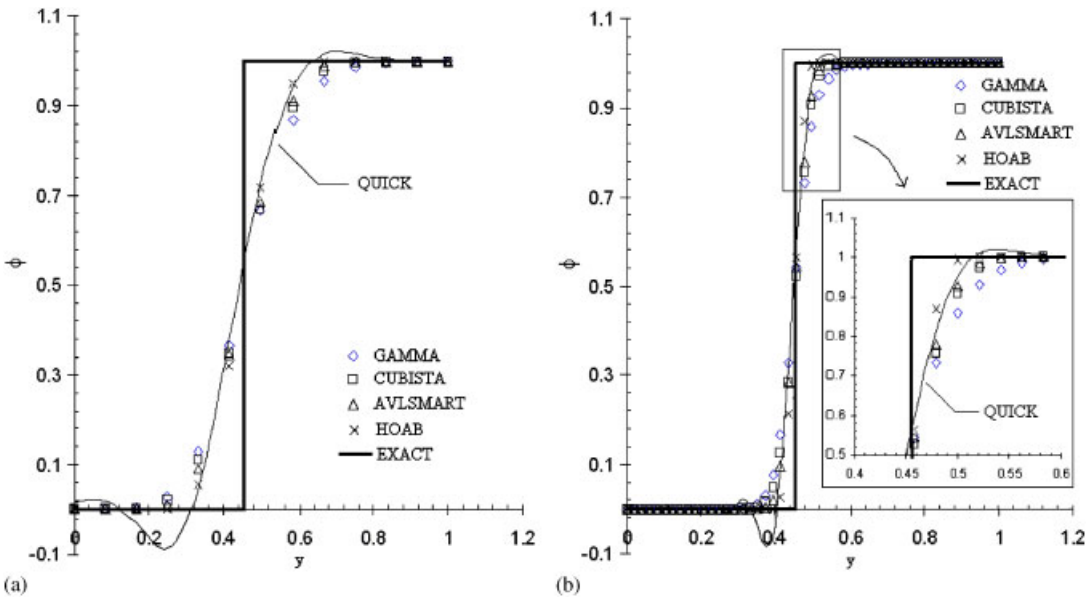

Figure 5. Resolutions of step profiles at various mesh spacing: (a) 12×12 control volumes; and (b) 48×48 control volumes.

The results on the coarsest and finest meshes are shown to dictate the marked variation of resolution properties at different mesh counts. The solution of QUICK is unsatisfactory, in view of its apparent oscillatory behaviour near the sharp front. Regarding the HOAB scheme, it is of interest to note that apart from its bounded behaviour, its capability to resolve the sharp profile is superior as compared to that of QUICK by examining the enlarged view to better show differences amongst the schemes. It can be seen that although AVLSMART, CUBISTA and GAMMA schemes are more diffusive as compared to QUICK, they tend to effectively remove the under- and overshoots of the unbounded QUICK scheme.

Figure 6 shows the error variation of different HR schemes at different mesh counts. The error is measured by

$$\text{Error} = \frac{1}{N}\sum_{n}^{N} |S_{n,\,\text{exact}} - S_{n,\,\text{predicted}}| \tag{29}$$

where S is the solution and N is the total number of grid points at line $x = 0.5$. As expected, HOAB possesses the least error and is the fastest in terms of rate of error reduction, followed by AVLSMART, CUBISTA and GAMMA.

To assess the robustness of the HR schemes, Table III compares the performance data relating to the computational costs of the tested schemes, obtained with all the four uniform grids. A converged solution is assumed when the maximum residual of the scalar variable is less than 1×10^{-7}. GAMMA is computationally more efficient than CUBISTA, AVLSMART and HOAB, especially in the case of fine mesh. An increase of relaxation factor may be helpful in accelerating the convergence as shown in Figure 7; however, HOAB shows a levelling out of the residual decay

DOI: 10.1002/fld

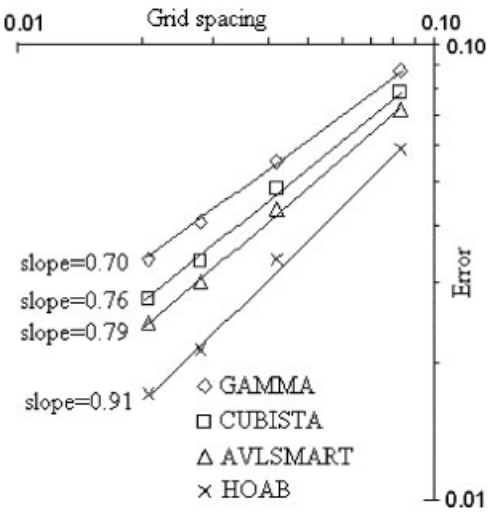

Figure 6. Estimated error versus grid spacing for convective passive scalar problem.

Table III. Performances of various differencing schemes for the calculation of passive scalar transport.

	Relaxation factor	0.50				0.60	0.30
	Mesh spacing	12×12	24×24	36×36	48×48	48×48	48×48
GAMMA	Iterations (total net	51	75	98	121	88	248
	CPU time, s)	(0.03)	(0.30)	(0.93)	(1.68)	(1.26)	(3.30)
CUBISTA	Iterations (total net	53	79	105	129	96	258
	CPU time, s)	(0.04)	(0.36)	(1.18)	(1.94)	(1.35)	(3.98)
AVL-SMART	Iterations (total net	63	92	117	139	103	283
	CPU time, s)	(0.05)	(0.41)	(1.33)	(2.23)	(1.53)	(4.05)
QUICK	Iterations (total net	80	110	138	163	123	325
	CPU time, s)	(0.03)	(0.25)	(0.64)	(1.28)	(1.02)	(2.48)
HOAB	Iterations (total net	103	154	214	255	—	452
	CPU time, s)	(0.09)	(0.80)	(2.91)	(4.85)		(7.68)

as the relaxation factor is increased to 0.6 and it is unable to provide a solution converged to the prescribed tolerance on the finest mesh (48×48). Similar observations have been found on coarser meshes and those performance data are not presented here for brevity purpose.

4.2. Compressible flow case: 2D transonic inviscid flow over a circular arc bump

The geometry for this problem is a 10% thick circular arc bump on the lower wall clearly defined in the work by Rincon and Elder [39]. It is reproduced here in Figure 8 for clarity purpose.

DOI: 10.1002/fld

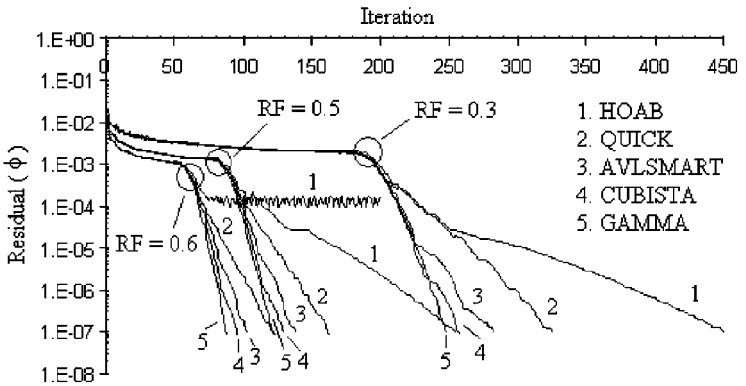

Figure 7. Effect on convergence histories at various relaxation factors (RFs) (Gauss–Seidel iterative method).

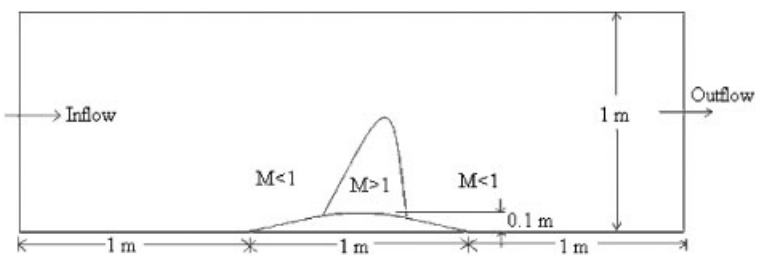

Figure 8. Geometric description of the circular arc bump.

At the inlet, the total pressure and the total temperature are fixed at 83858.92 Pa and 327.34 K, respectively, and the velocity vector is assumed to be normal to the inlet boundary edge. At the exit, static pressure is prescribed at 61800.00 Pa, which corresponds to the inlet Mach number of about 0.675. The calculations are performed on five consecutively refined unstructured triangular meshes (average mesh spacing = 100, 80, 50, 40 and 30 mm) in order to evaluate the reduction of error with mesh refinement of the various HR schemes. The convergence issues with different NVF limiters are dealt first, followed by the accuracy study.

Figure 9 compares the time-evolution of the residuals of density as a function of multigrid cycle for different HR schemes. A converged solution is assumed when the maximum residual of the density falls below 1×10^{-6} and all the convergence histories displayed in Figure 9 have been obtained with a Courant number (Co) of 0.3 at an average mesh spacing of 30 mm. Assessment of Figure 9 indicates that GAMMA, CUBISTA and AVLSMART schemes converge at about the same rate, while GAMMA showing the rapidest decay of residual amongst the others. The HOAB scheme, however, is unable to converge to the prescribed tolerance. In view of this, the authors investigate next the effect of the size of the time step on the iterative convergence property for the HOAB scheme. Results are presented in Figure 10, showing the decay of residuals for a time step ranging from Co = 0.1 to 0.5; the corresponding predicted minimum pressure immediately before the compression shock are given in Figure 11. It is found that in this case, the iterative convergence

DOI: 10.1002/fld

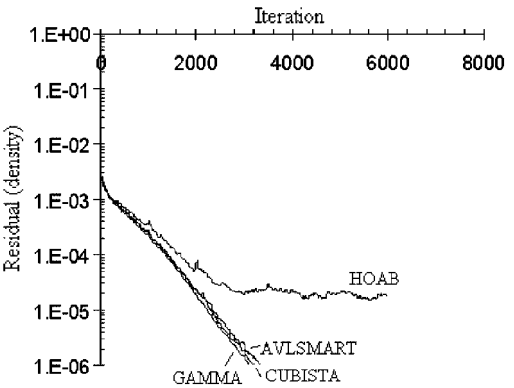

Figure 9. Convergence histories of various HR schemes at Courant number (Co) = 0.3. Average mesh spacing = 30 mm.

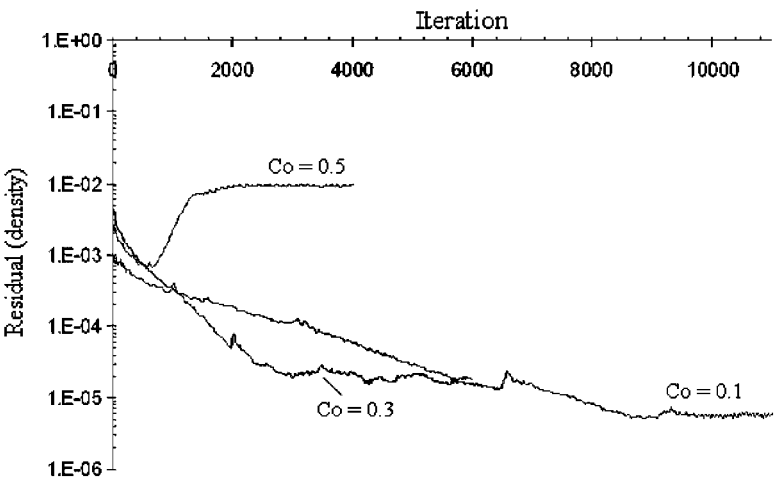

Figure 10. Influence of Courant number (Co) of the decay of the residual of density for HOAB scheme. Average mesh spacing = 30 mm.

behaviour of the HOAB scheme is improved with smaller time steps. By looking simultaneously to the evolution of the residuals and of the predicted minimum pressure immediately before the compression shock, the residuals are still decaying to a certain lower level when the solution field has already achieved a certain stabilized stage. Inspection of Figure 11 shows that the time-asymptotic solutions for the cases employing different time steps are essentially unique; however, in terms of robustness, it is desirable to devise a scheme that is able to achieve rapid decaying of residuals without relying heavily on the size of the time-step. Also, based on the history plots, it is safe to declare that the solution is time asymptotic when the residual has reached to an adequate non-varying level.

DOI: 10.1002/fld

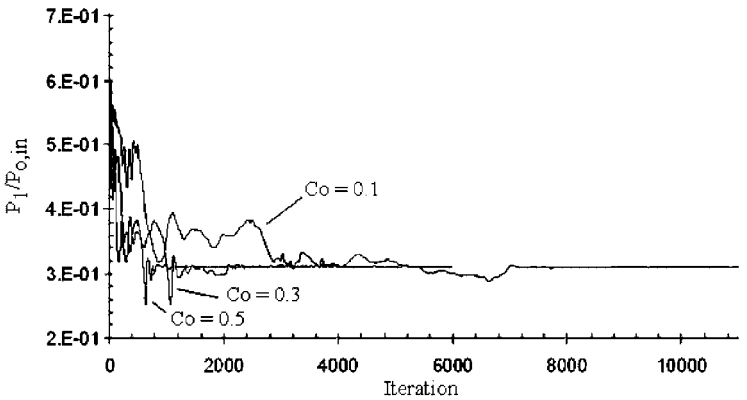

Figure 11. Influence of Courant number (Co) of the steady state result predicted by HOAB. $P_1 = P_{\min}$ at upstream of the shock along the lower wall. Average mesh spacing = 30 mm.

Table IV. Mach-peaks before the compression shock under steady-state condition.

Average mesh spacing (mm)	100	80	50	40	30
HOAB	1.246	1.265	1.315	1.363	1.373
AVLSMART	1.196	1.247	1.310	1.331	1.365
CUBISTA	1.181	1.227	1.289	1.308	1.334
GAMMA	1.134	1.180	1.260	1.275	1.324

$M_{ref} = 1.385$ (cf. Reference [38, Figure 6(a)]).

Table IV shows the comparison of Mach-peak immediately before the shock predicted by using various HR schemes on different meshes. The reference value reported by Ni [40] has been used in the present study for comparison purpose. The estimated errors for the HR schemes, taken as the difference between the predicted Mach-peak and the reference value versus the grid spacing, are presented in Figure 12. Only on the highest mesh count, all the HR schemes have successfully produced results with an error band within 5%, while prediction by HOAB differs by only 0.8% from the reference value. Again, HOAB experiences the fastest decay of the estimated error as compared to the others. The resolutions of the compression shocks are presented in Figure 13 for various differencing schemes on the finest computational meshes. HOAB scheme, due to its least amount of diffusion level (highest NEBF), perfectly resolves the shock discontinuity, followed by AVLSMART, CUBISTA and GAMMA.

4.3. Incompressible flow case: 3D lid-driven laminar flow in a cubic cavity

The test problem considered here is the 3D lid-driven laminar flow in a cubic cavity. The geometric description of the cubic cavity is illustrated in Figure 14. Despite its relatively simple geometry, driven flow in a cavity has been vastly used as a test case due to its complex flow pattern. The Reynolds number is defined as $Re = UL/v$. A constant kinematic viscosity (v) of 1×10^{-5} m^2/s

DOI: 10.1002/fld

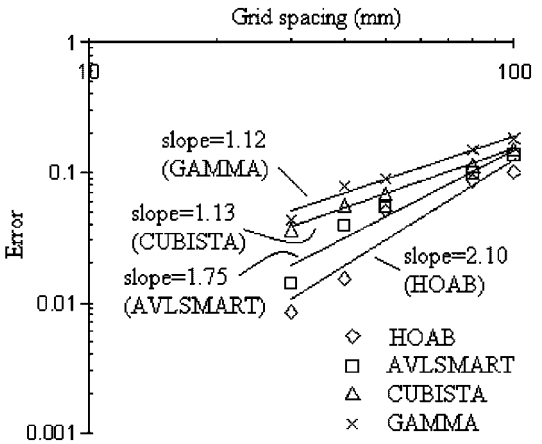

Figure 12. Estimated error in the Mach-peak before the shock versus average mesh spacing (mm).

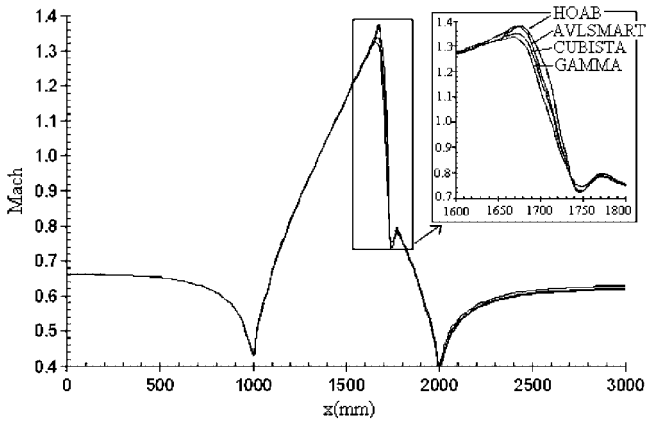

Figure 13. Mach distributions at steady-state condition along the bottom wall with arc at inlet Mach of 0.675. Average mesh spacing = 30 mm.

is prescribed in the entire flow field, $L = 1$ m is assumed and the lid velocity, U is adjusted in such a way that the prescribed Reynolds number is satisfied.

Calculation is firstly carried out for a Reynolds number of 400 at four mesh counts, in which the 3D solutions of Shu *et al*. [41] using the Lattice–Boltzmann method is available. The 3D effect of the flow has been reported by Shu *et al*. [41]. Figures 15 and 16 display the u-velocity profiles on L1 and w-velocity profiles on L2, respectively, on the plane $y = 0.5$ m predicted on the computational meshes consist of $40 \times 40 \times 40$ control volumes. At this Reynolds number, the predictions from the HR schemes show remarkably good agreement with the reference solution, while the HOAB scheme again yields the most accurate result among the others. By closely examining the velocity plots,

DOI: 10.1002/fld

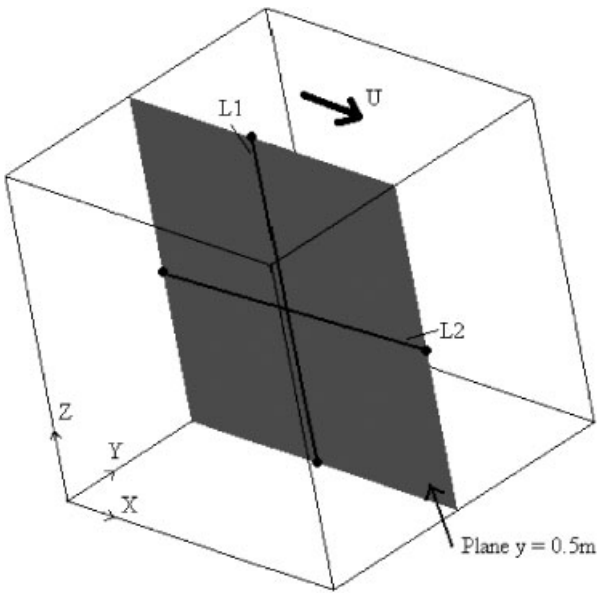

Figure 14. Geometric description of 3D lid-driven flow in a cubic cavity. L1 ($x = 0.5$ m) and L2 ($z = 0.5$ m) are constructed for presentation of results.

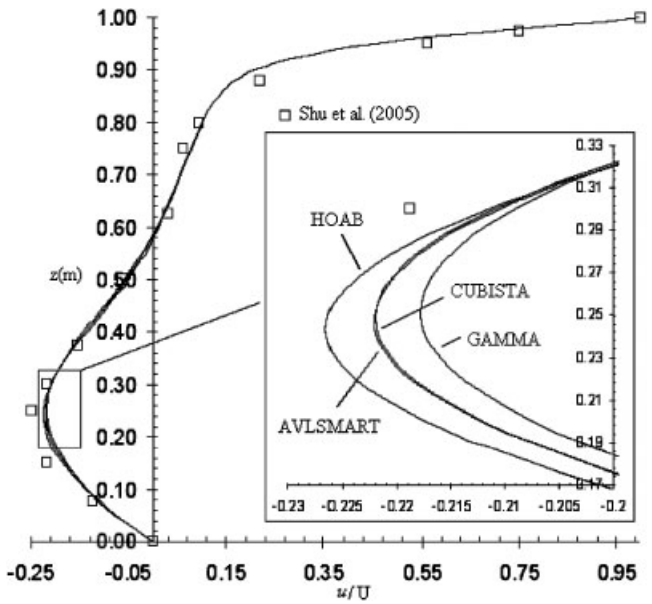

Figure 15. u-velocity profiles along L1 for 3D lid-driven cavity flow. $Re = 400$. Mesh $= 40 \times 40 \times 40$.

DOI: 10.1002/fld

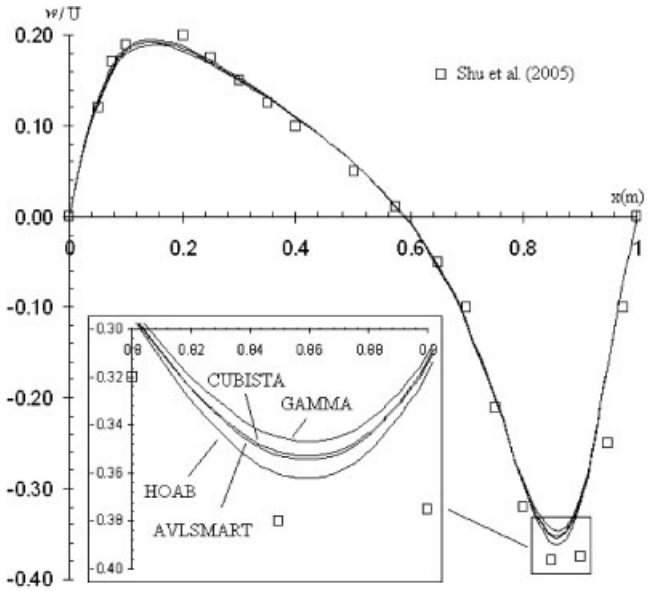

Figure 16. w-velocity profiles along L2 for 3D lid-driven cavity flow. $Re = 400$. Mesh $= 40 \times 40 \times 40$.

it shows that the predictions from CUBISTA represent very closely with those from AVLSMART, with closer agreement to the HOAB solution for the latter. GAMMA scheme tends to underpredict the velocity peaks in both the u- and w- profiles. The degree of deviation of the u-velocity peak for various HR schemes have been quantitatively measured for different mesh counts and shown in Figure 17 where the reference value (dimensionless u-velocity) is taken as -0.25 (cf. Reference [41]). Both AVLSMART and CUBISTA schemes experience a similar decaying rate of error while the reduction of error is again the fastest for HOAB scheme.

To assess the computational cost as well as the iterative convergence property of the HR schemes, Table V compares the number of iterations and the total net CPU time required by various schemes for the vanishing of residuals (residual of $u < 1 \times 10^{-6}$). HOAB scheme, although is proven to be very accurate, suffering from degradation of iterative convergence property as it shows a levelling out of residual decay without achieving the convergence levels as those of UD and other HR schemes (see Figure 18). GAMMA scheme, despite the fact that it is relatively diffusive as compared to other HR schemes, is more efficient in terms of CPU time saving. Also, it is worth to mention here that CUBISTA and AVLSMART require only 3–4% more CPU time than GAMMA at the finest mesh level, and meanwhile the former schemes have shown better accuracy as compared to the latter.

The calculations are then performed for higher Reynolds number ($Re = 1000$). Since no experimental/reference data are available, the solution of QUICK is taken as reference and compared to those of other HR schemes. The QUICK solutions on meshes $30 \times 30 \times 30$ and $40 \times 40 \times 40$ are seen to be almost identical, and thus the solution is essentially grid-independent for this reference scheme. Besides the above calculations which mainly focus on the assessments of the four HR schemes, computations are carried out for the tested HR schemes and their

DOI: 10.1002/fld

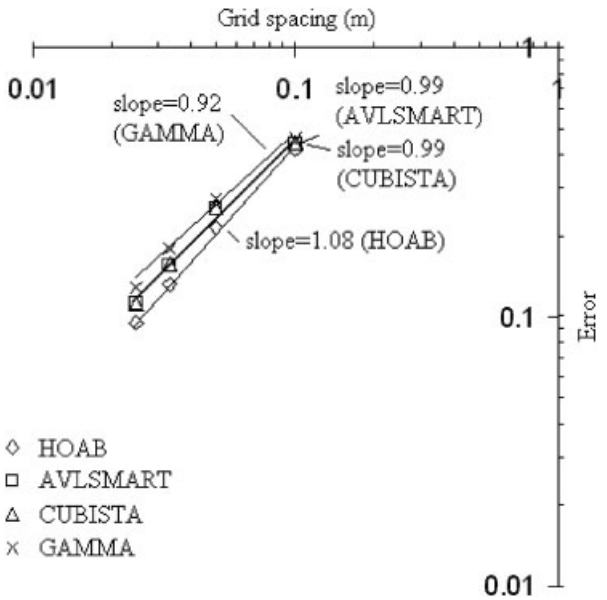

Figure 17. Estimated error in the negative peak of u-velocity at L1 versus grid spacing (m).

Table V. Performances of different HR schemes at various mesh counts for 3D computation of lid-driven cavity flow ($Re = 400$).

Mesh	$40 \times 40 \times 40$ Iterations (total net CPU time, s)	$30 \times 30 \times 30$ Iterations (total net CPU time, s)	$20 \times 20 \times 20$ Iterations (total net CPU time, s)	$10 \times 10 \times 10$ Iterations (total net CPU time, s)
HOAB	246 (363.23)	—	—	—
AVL-SMART	240 (357.39)	164 (101.80)	104 (16.77)	36 (0.72)
CUBISTA	239 (354.33)	163 (101.56)	104 (16.73)	36 (0.72)
GAMMA	234 (344.08)	159 (98.53)	101 (16.13)	35 (0.67)
UD	180 (177.41)	122 (51.41)	78 (8.45)	29 (0.41)

corresponding BD schemes by Peric [31] to investigate both the solution accuracy and computational cost of the linear- and non-linear blending schemes. Table VI gives the performance data in terms of computational costs of various HR schemes and the BD schemes on mesh $20 \times 20 \times 20$.

DOI: 10.1002/fld

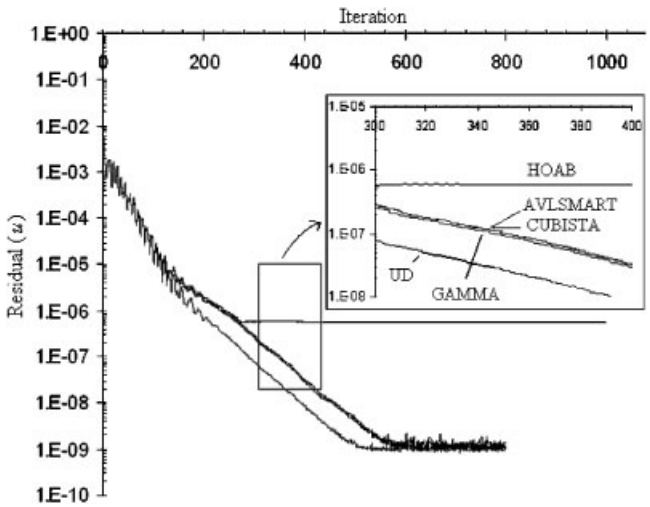

Figure 18. Convergences histories of various HR schemes for computation of 3D lid-driven cavity flow. $Re = 400$. Mesh $= 40 \times 40 \times 40$.

Table VI. Performances of the high-resolution, BD (UD + CD) and QUICK schemes for the computation of 3D lid-driven flow ($Re = 1000$; mesh spacing $20 \times 20 \times 20$).

	0.7500		0.9341		0.9939		
BF/NEBF	GAMMA	BD (75.00)*	CUBISTA	BD (93.41)*	AVL-SMART	BD (99.39)*	QUICK
a	127	132	153	182	159	234	249
b	20.41	20.17	24.63	27.75	25.52	35.58	38.13

a = number of iterations; b = total net CPU time (s).
*=% of CD. BF = blending factor, NEBF = net effective blending factor.

For GAMMA scheme, it is slightly less efficient ($\sim$ 1% more CPU time) than its corresponding BD scheme computationally; however, for schemes of higher NEBF (CUBISTA and AVLSMART), there is a marked saving of computational cost while employing the HR schemes as compared to their corresponding BD schemes. To check on their accuracies, Figure 19 compares the w-velocity plots at L2 for various schemes. Interestingly enough, the results show not only that both CUBISTA and AVLSMART require less amounts of computational efforts to reach convergence, they can attain even better accuracies as compared to their corresponding BD schemes with closer representations of the formers to the QUICK solution on the same mesh ($20 \times 20 \times 20$). This finding again appreciates that in an attempt to search for a differencing scheme that is promising in terms of iterative convergence property as well as accuracy, a composite blending function (γ-functions in NVD) being constructed at different flow regions is, without further thoughts, a necessity.

DOI: 10.1002/fld

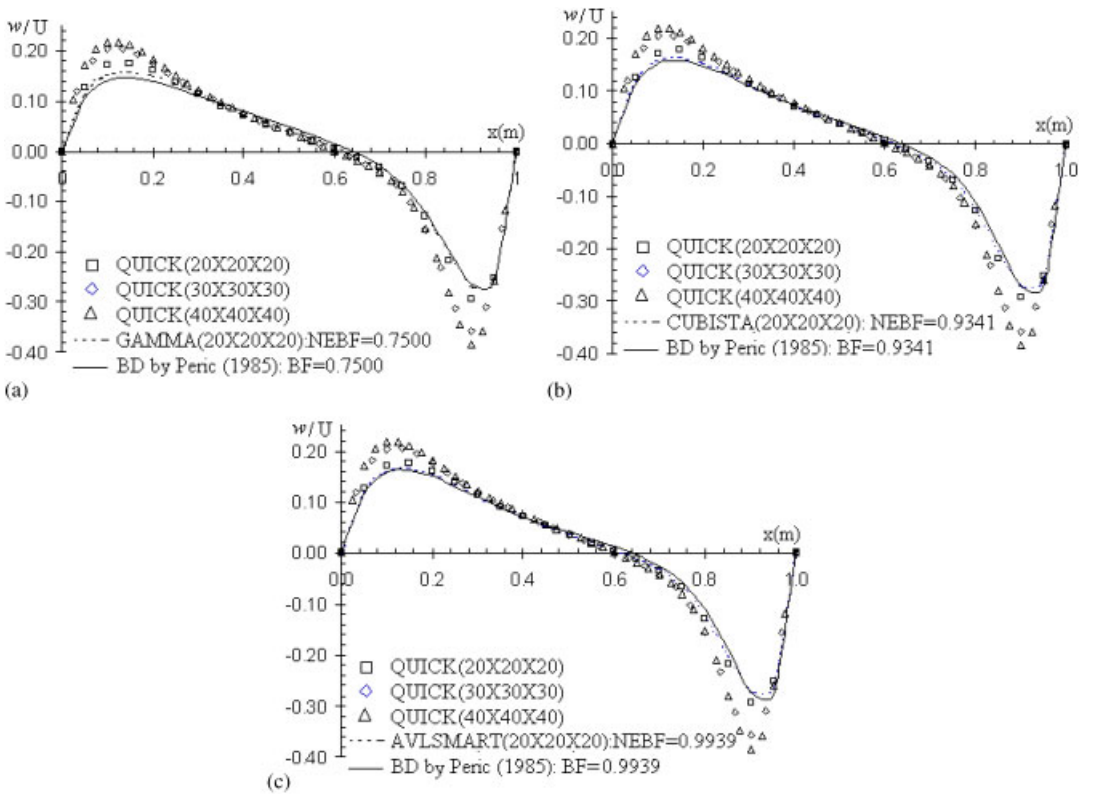

Figure 19. w-velocity profiles at L2 for 3D lid-driven cavity flow. $Re = 1000$. Mesh $= 20 \times 20 \times 20$ for blended differencing (BD) and HR schemes: (a) NEBF and blending factor (BF) $= 0.7500$; (b) NEBF and blending factor (BF) $= 0.9341$; and (c) NEBF and blending factor (BF) $= 0.9939$.

5. CONCLUSION

A comparison in terms of numerical accuracy, computational cost as well as iterative convergence property of the recently developed high-resolution (HR) schemes, namely HOAB, AVLSMART, CUBISTA and GAMMA, has been made. All the HR schemes have been formulated with a unified class of dual-formulation denoted as the γ-family of schemes, which are able to achieve higher-order approximations by expressing the blending factor as a function of compact normalized variables. Contrary to the χ-family of schemes that use distinct base schemes, consistency is enforced by employing central differencing (CD) as the base scheme for the construction of all HR schemes, thus allowing straightforward implementations of HR schemes particularly on unstructured meshes. Using the proposed numerical framework of γ-family of schemes, the net effective blending factor (NEBF) has been derived and it has been proven to be an effective tool in revealing quantitatively the relative diffusion levels (hence relative accuracies) inherited in the present HR schemes under investigation. In the present study, HOAB is the most accurate scheme among all at the expense of degradation in iterative convergence property and hence computational cost owing to its highest

DOI: 10.1002/fld

NEBF, followed by AVLSMART, CUBISTA and GAMMA. GAMMA scheme, although formally one order of accuracy less than CUBISTA, AVLSMART and HOAB, its result shows no substantial difference with those of the higher-order schemes particularly for low-*Re* flow. Furthermore, due to the fact that its NVF characteristics lines reside closer to the UD line (lowest NEBF amongst the HR schemes considered), GAMMA scheme is computationally more efficient than the other three schemes, especially in the case of fine grids. For HR schemes that employ third-order accurate schemes at smooth flow region, it has been found that CUBISTA is nearly as robust as the second-order GAMMA; however, its accuracy is less superior as compared to those of AVLSMART and HOAB, due to its lowest NEBF amongst the studied third-order HR schemes.

ACKNOWLEDGEMENTS

This project is funded by the Ministry of Science Technology and Innovation (MOSTI), Malaysia under the IRPA Grant No. 09-99-03-0013-EA001 and UNITEN Internal Research Grant No. J510010026.

REFERENCES

1. Patankar SV. *Numerical Heat Transfer and Fluid Flow*. Hemisphere: Washington, DC, 1980.
2. Spalding DB. A novel finite-difference formulation for differential expressions involving both first and second derivatives. *International Journal for Numerical Methods in Engineering* 1972; **4**:551–559.
3. Raithby GD. Skew upwind differencing schemes for problems involving fluid flow. *Computer Methods in Applied Mechanics and Engineering* 1976; **9**:153–164.
4. Darwish M, Moukalled F. A new approach for building bounded skew-upwind schemes. *Computer Methods in Applied Mechanics and Engineering* 1996; **129**:221–233.
5. Gaskell PH, Lau AKC. Curvature-compensated convective transport: smart, a new boundedness-preserving transport algorithms. *International Journal for Numerical Methods in Fluids* 1988; **8**:617–641.
6. Warming RF, Beam RM. Upwind second order difference schemes and applications in aerodynamic flow. *AIAA Journal* 1976; **14**:1241–1249.
7. Leonard BP. A stable and accurate convective modeling procedure based on quadratic upstream interpolation. *Computer Methods in Applied Mechanics and Engineering* 1979; **19**:59–98.
8. Agarwal RK. A third order accurate upwind scheme for Navier Stokes solutions in three dimensions. In *Computers in Flow Prediction and Fluid Dynamics Experiments*, Ghia KN, Mueller TJ, Patel BR (eds). ASME Winter Meeting: Washington, 1981; 73–82.
9. Harten A. High resolution schemes for hyperbolic conservation laws. *Journal of Computational Physics* 1983; **49**:357–393.
10. Roe PL. Large scale computations in fluid mechanics, part 2. In *Lectures in Applied Mathematics*, vol. 22. Springer: Berlin, 1985; 163–193.
11. Sweby PK. High resolution schemes using flux limiters for hyperbolic conservation laws. *SIAM Journal on Numerical Analysis* 1984; **21**:995–1011.
12. Van Leer B. Towards the ultimate conservative difference scheme V, a second order sequel to Godunov's method. *Journal of Computational Physics* 1977; **23**:101–136.
13. Chan KI, Ng EYK. Modified distribution-formula scheme for unstructured adaptive Navier–Stokes solvers. *International Journal of Computational Methods* 2005; **2**:1–26.
14. Leonard BP. The ULTIMATE conservative difference scheme applied to unsteady one-dimensional advection. *Computer Methods in Applied Mechanics and Engineering* 1991; **88**:17–74.
15. Zijlema M, Wesseling P. Higher order flux-limiting methods for steady-state, multidimensional, convection-dominated flow. *Report 95-131*, Delft University of Technology, 1995.
16. Zhu J, Rodi W. A low dispersion and bounded convection scheme. *Computer Methods in Applied Mechanics and Engineering* 1991; **92**:87–96.
17. Jasak H, Weller H, Gosman AD. High resolution NVD differencing scheme for arbitrarily unstructured meshes. *International Journal for Numerical Methods in Fluids* 1999; **31**:431–449.

DOI: 10.1002/fld

18. Song B, Liu GR, Lam KY, Amano RS. On a higher-order bounded discretization scheme. *International Journal for Numerical Methods in Fluids* 2000; **32**:881–897.
19. Song B, Liu GR, Amano RS. Applications of a higher-order bounded numerical scheme to turbulent flow. *International Journal for Numerical Methods in Fluids* 2001; **35**:371–394.
20. Przulj V, Basara B. Bounded convection schemes for unstructured grids. *AIAA Paper No. 2001-2593*, *AIAA Computational Fluid Dynamics Conference*, Anaheim, California, U.S.A., 2001.
21. Hou PL, Tao WQ, Yu MZ. Refinement of the convective boundedness criterion of Gaskell and Lau. *Engineering Computations* 2003; **20**:1023–1043.
22. Alves MA, Oliveira PJ, Pinho FT. A convergent and universally bounded interpolation scheme for the treatment of advection. *International Journal for Numerical Methods in Fluids* 2003; **41**:47–75.
23. Darwish M, Moukalled F. The χ-schemes: a new consistent high-resolution formulation based on the normalized variable methodology. *Computer Methods in Applied Mechanics and Engineering* 2003; **192**:1711–1730.
24. Wei JJ, Yu B, Tao WQ, Kawaguchi Y, Wang HS. A new high-order accurate and bounded scheme for incompressible flow. *Numerical Heat Transfer*, *Part B* 2003; **43**:19–41.
25. Woodfield PL, Suzuki K, Nakabe K. A simple strategy for constructing bounded convection schemes for unstructured grid. *International Journal for Numerical Methods in Fluids* 2004; **46**:1007–1024.
26. Leonard BP. Simple high-accuracy resolution program for convective modeling of discontinuities. *International Journal for Numerical Methods in Engineering* 1988; **8**:1291–1318.
27. Chakravarthy SR, Osher S. High-resolution applications of the OSHER upwind scheme for the Euler equations. *AIAA Paper No. 83-1943*, *AIAA 6th Computational Fluid Dynamics Conference*, Danvers, MA, July 1983.
28. Fromm JE. A method for reducing dispersion in convective difference schemes. *Journal of Computational Physics* 1968; **3**:176–189.
29. Khosla PK, Rubin SG. A diagonally dominant second-order accurate implicit scheme. *Computers and Fluids* 1974; **2**:207–209.
30. Li ZY, Tao WQ. A new stability-guaranteed second-order difference scheme. *Numerical Heat Transfer*, *Part B* 2002; **42**:349–365.
31. Peric M. A finite volume method for the prediction of three-dimensional fluid flow in complex ducts. *Ph.D. Thesis*, Imperial College, University of London, U.K., 1985.
32. Ng KC, Yusoff MZ, Ng EYK. Multigrid solution of Euler equations using high-resolution NVD differencing scheme for unstructured meshes. *Progress in Computational Fluid Dynamics* 2006, in press.
33. Ng KC. Multigrid solution using high-resolution NVF differencing scheme for solution-adaptive unstructured meshes. *Ph.D. Thesis*, College of Engineering, Universiti Tenaga Nasional, Malaysia, 2006.
34. Jameson A, Schmidt W, Turkel E. Numerical solutions of the Euler equations by finite volume methods using Runge–Kutta time stepping schemes. *AIAA Paper No. 81-1259*, 1981.
35. Jameson A. Transonic flow calculations. *MAE Report 1651*, MAE Department, Princeton University, U.S.A., 1983.
36. Zhu J. On the higher-order bounded discretization schemes for finite volume computations of incompressible flows. *Computer Methods in Applied Mechanics and Engineering* 1992; **98**:345–360.
37. Rhie CM, Chow WL. A numerical study of the turbulent flow past an isolated airfoil with trailing edge separation. *AIAA Journal* 1983; **21**:1525–1532.
38. Jasak H. Error analysis and estimation for the finite volume method with applications to fluid flows. *Ph.D. Thesis*, Imperial College, University of London, U.K., 1996.
39. Rincon J, Elder R. A high-resolution pressure-based method for compressible flows. *Computers and Fluids* 1997; **26**:217–231.
40. Ni RH. A multiple grid scheme for solving the Euler equations. *AIAA Journal* 1982; **20**:1565–1571.
41. Shu C, Niu XD, Peng Y, Chew YT. Taylor series expansion- and least square-based Lattice Boltzmann method: an efficient approach for simulation of incompressible viscous flow. *Progress in Computational Fluid Dynamics* 2005; **5**:27–36.

DOI: 10.1002/fld